Angular phase shift in polarization-angle dependence of microwave-induced magnetoresistance oscillations

Han-Chun Liu, Rasanga L. Samaraweera, and R. G. Mani
Department of Physics and Astronomy, Georgia State University, Atlanta, Georgia 30303, USA

C. Reichl and W. Wegscheider
Laboratorium für Festkörperphysik, ETH Zürich, CH-8093 Zürich, Switzerland

(Received 22 July 2016; revised manuscript received 12 September 2016; published 28 December 2016)

We examine the microwave frequency (f) variation of the angular phase shift, θ_0, observed in the polarization-angle dependence of microwave-induced magnetoresistance oscillations in a high-mobility GaAs/AlGaAs two-dimensional electron system. By fitting the diagonal resistance R_{xx} versus θ plots to an empirical cosine square law, we extract θ_0 and trace its quasicontinuous variation with f. The results suggest that the overall average of θ_0 extracted from Hall bar device sections with length-to-width ratios of $L/W = 1$ and 2 is the same. We compare the observations with expectations arising from the "ponderomotive force" theory for microwave radiation-induced transport phenomena.

DOI: 10.1103/PhysRevB.94.245312

I. INTRODUCTION

Zero resistance states (ZRS) and associated radiation-induced magnetoresistance oscillations observed in two-dimensional electron systems (2DESs) based on GaAs/AlGaAs heterostructures subjected to a perpendicular magnetic field and microwaves/millimeter-wave/terahertz radiation reveal extraordinary physical properties [1,2]. Such radiation-induced magnetoresistance oscillations display a "1/4-cycle phase shift" with periodicity in $1/B$, so that the oscillatory minima emerge at $B = [4/(4j+1)]B_f$, where $B_f = 2\pi f m^*/e$, f is the microwave frequency, m^* is the effective electron mass, and $j = 1,2,3,\ldots$ [1]. Numerous fascinating features of associated phenomena and transport in high-mobility 2DESs have been studied over the past decade [1–31], including, for example, the nonlinear increase in the amplitude of oscillatory magnetoresistance with microwave power [15,22,25], and the linear- and circular-polarization dependence of radiation-induced oscillations [6,17,19,22,24–27]. At the same time, a number of theories have also been proposed to describe the physical mechanisms associated with radiation-induced transport [32–60], including the displacement model [9,32–34,41,43,47,57,60], the nonparabolicity model [35], the inelastic model [42], the radiation-driven electron-orbit model [44,45,48,49,52,55], and the "ponderomotive force" model [50].

An interesting and unexpected development was the identification of the remarkable sensitivity of the amplitude of oscillatory magnetoresistance to the polarization angle of linearly polarized microwave radiation [17,19,22,24–27] complementing the circular polarization work [6,27,46]. Here, Ramanayaka *et al.* demonstrated a sinusoidal-curved variation of the amplitude of the oscillatory magnetoresistance with the microwave polarization angle at moderate radiation power [19]. It turns out that the predictions of the displacement model, the nonparabolicity model, and the radiation-driven electron-orbit model for $\gamma < \omega$, where γ is a damping factor and $\omega = 2\pi f$, are roughly in agreement with the observed experimental results in Refs. [32–35,40,41,43,44,47,52,57,60]. Empirically, the sinusoidal variation in oscillatory magnetoresistance with the polarization angle can be expressed by $R_{xx}(\theta) = A \pm C\cos^2(\theta - \theta_0)$, where R_{xx} is the diagonal magnetoresistance, θ is the microwave polarization angle, θ_0 is the phase shift, and the plus and minus signs correspond to the oscillatory maxima and minima, respectively [19,22,24–27]. Previous studies carried out at a set of discrete frequencies have examined the question of whether θ_0 is f- or B-dependent [19,22,24–27]. Meanwhile, some theories have successfully reproduced sinusoidal-curved variations in R_{xx} versus θ [53,55]. However, the predicted behavior of θ_0 has not been observed experimentally. Thus, at present, the origin and evolution of the phase shift θ_0 is still an unresolved issue in this field.

As mentioned earlier, previous studies of the phase-shift angle θ_0 have been carried out by changing θ continuously at oscillatory extrema of R_{xx} at a discrete set of specific f, and extracting θ_0 by fitting to an empirical cosine square rule [19,22,24–27]. In this approach, however, the evolution of θ_0 between the measured f was unknown. Thus, one might wonder if θ_0 is extremely f-sensitive and includes wild variations in the phase shift between the radiation frequencies where the measurements were carried out, or if the phase shift was sensitive to sample geometric factors such as the length-to-width ratio of the Hall bars. In this paper, therefore, the quasicontinuous evolution of the phase shift θ_0 extracted from R_{xx} versus θ traces of the radiation-induced magnetoresistance oscillations at a set of six oscillatory extrema is examined over the frequency band $36 \leqslant f \leqslant 40$ GHz for Hall-bar sections for device width-to-length ratios, $L/W = 1$ and 2. That is, the extracted θ_0 is presented over an f-band with nearly continuous change in f. The results indicate that the θ_0 extracted from the $L/W = 1$ Hall-bar section, $\theta_{0,1}$, shows less f-dependence than that extracted from the $L/W = 2$ Hall-bar section, $\theta_{0,2}$. However, $\theta_{0,1}$ exhibits a remarkably similar overall average to $\theta_{0,2}$ over $36 \leqslant f \leqslant 40$ GHz. The results are interesting because they show that the proximity of contacts is not a factor influencing the observed phase shift, unlike expectations based on the "ponderomotive force"

theory [50]. On the other hand, the results are not incompatible with the displacement and radiation-driven electron orbit theories [32–34,40,44,45,48,49,52,55].

II. EXPERIMENT AND RESULTS

For this study, Hall-bar type samples with alloyed gold-germanium contacts were fabricated by optical lithography from molecular-beam-epitaxy (MBE) -grown GaAs/AlGaAs heterojunctions with electron density $n = 3.3 \times 10^{11}$ cm^{-2} and mobility $\mu = 14 \times 10^6$ cm^2 V^{-1} s^{-1} at $T = 1.5$ K. Thus, the specimens examined here include a noticeably higher mobility compared to the specimens examined in some of our previous studies [16,17,19,19,22,24–27], although not quite as high as in the earlier work [1,3–5,10,12,15]. 200-μm-wide Hall-bar sections were measured using the four-terminal lock-in techniques with ac current, I, applied along the length of the device, as in Fig. 1(a). The Hall-bar device is situated at the bottom end of a circular waveguide through which linear-polarized microwaves with a rotatable polarization at polarization angle θ are transmitted onto the specimen [19,22,24–27]. The polarization angle θ increases clockwise, as indicated in Fig. 1(a) with respect to the Hall-bar axis. The diagonal magnetoresistances, $R_{xx,1}$ and $R_{xx,2}$, which represent the extracted magnetoresistance for the $L/W = 1$ and 2 sections of the Hall bar, respectively, are measured simultaneously during experiment. Further, although the calibration of the microwave polarization angle θ is carried out *a priori* by setting $\theta = 0$ when the microwave electric field is oriented along the Hall-bar axis direction [19,22,24–27], an Allen-Bradley (ABR) carbon resistance sensor with a strong negative temperature coefficient, i.e., $dR_{\rm ABR}/dT \leqslant 0$, at liquid-helium temperatures, was placed next to the Hall-bar specimen [4,5,22] for the sake of *in situ* measurement of θ_0 and the independent detection of microwave polarization rotation at the sample location. Although the carbon resistor was not used for this purpose before, it is able to detect microwave polarization rotation with respect to its preferred axis, i.e., $\theta = 90^\circ$ in Fig. 1(a), as a changed heating effect, with maximal heating occurring when the microwave polarization is along the axis of the carbon resistor.

Figure 1(b) shows strong radiation-induced magnetoresistance oscillations in $R_{xx,1}$ and $R_{xx,2}$ versus B at $f = 38$ GHz, the frequency we call mid-f. Observed asymmetries in the R_{xx} of Fig. 1(b) under B-field reversal could be due to doping gradients [31]. In the figure, we define the first (second) peak and the first valley on the positive side of B as $P1+$ ($P2+$) and $V1+$, respectively [19,22,24–27]. Likewise, $P1-$, $V1-$, and $P2-$ are labels utilized to identify extrema on the negative side of the B axis. f-sweep measurements are performed at angles ranging from $\theta = 0^\circ$ to 360° at 10° increments over the frequency band $36 \leqslant f \leqslant 40$ GHz at the six labeled oscillatory extrema. It is well known that the B-positions of oscillatory extremal R_{xx} are linearly proportional to f [1–30]. During the f-sweep measurements, the B of oscillatory extrema will therefore vary with f. It is therefore understood that the θ_0 can not only be f-dependent but also B-dependent [19,25,26]. To reduce the B effect on θ_0, the B of oscillatory extrema are fixed for the values appropriate for the mid-f, i.e., the B values for the oscillatory extrema are chosen from the R_{xx} versus B traces at 38 GHz. According to the linear relationship between B and f, ≈ 4.8 mT shift can occur in a 2 GHz band with respect to mid-f, which is only an $\approx 5\%$ change in B. Therefore, given the breadth of the oscillatory extrema, the B effect on θ_0 is neglected in f-sweep measurements presented here.

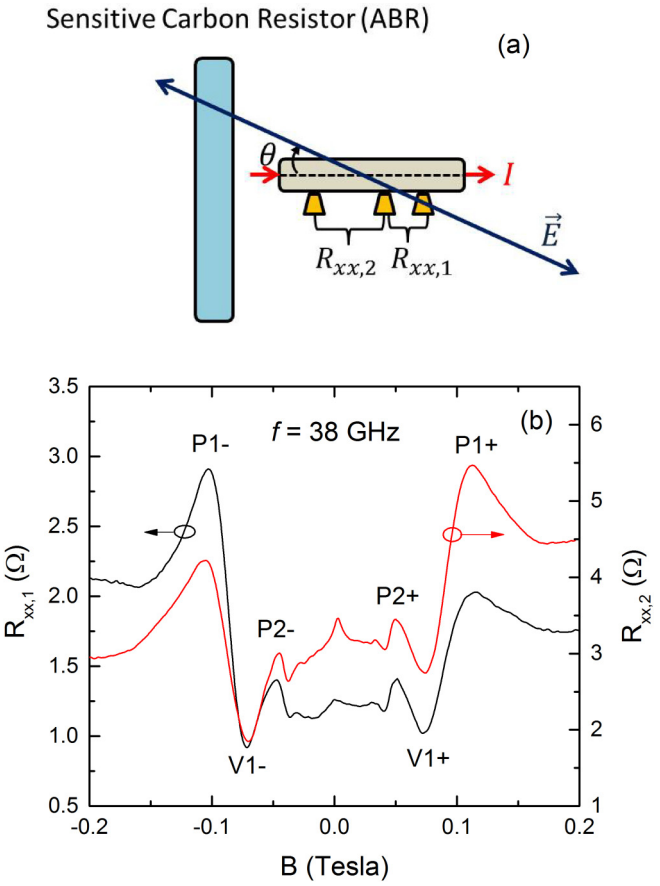

FIG. 1. (a) This schematic shows the relative orientation of the GaAs/AlGaAs heterojunction and the carbon resistor (ABR), which were subjected to rotatable linearly polarized radiation at the polarization angle θ with respect to the Hall bar axis. θ increases in the clockwise direction. Here, $R_{xx,1}$ and $R_{xx,2}$ represent the diagonal resistance measured in sections with length-to-width ratios $L/W = 1$ and 2, respectively. (b) This panel illustrates $R_{xx,1}$ and $R_{xx,2}$ vs B, which show observable radiation-induced magnetoresistance oscillations at $f = 38$ GHz. The oscillatory extrema are labeled as $P1+$, $V1+$, $P2+$, $P2-$, $V1-$, and $P1-$. The B-field positions of these extrema are tracked over the $36 \leqslant f \leqslant 40$ GHz band in this paper.

To verify that the variation of θ_0 reported by the specimen is not caused by uncharacterized polarization rotation by the experimental apparatus, we utilized the carbon resistor (ABR) next to the specimen to determine the microwave polarization orientation near the specimen during measurements. Because the preferred axis of ABR is set at $\theta = 90^\circ$, the $R_{\rm ABR}$ reading is highest at $\theta = 0^\circ$ and lowest at $\theta = 90^\circ$. Figure 2(a) shows a normalized $R_{\rm ABR}$ color plot of f versus θ over $36 \leqslant f \leqslant 40$ GHz with $0^\circ \leqslant \theta \leqslant 360^\circ$ at $V1-$. A bluish color represents lower resistance, and a reddish color represents higher resistance. The result demonstrates that higher normalized $R_{\rm ABR}$ is

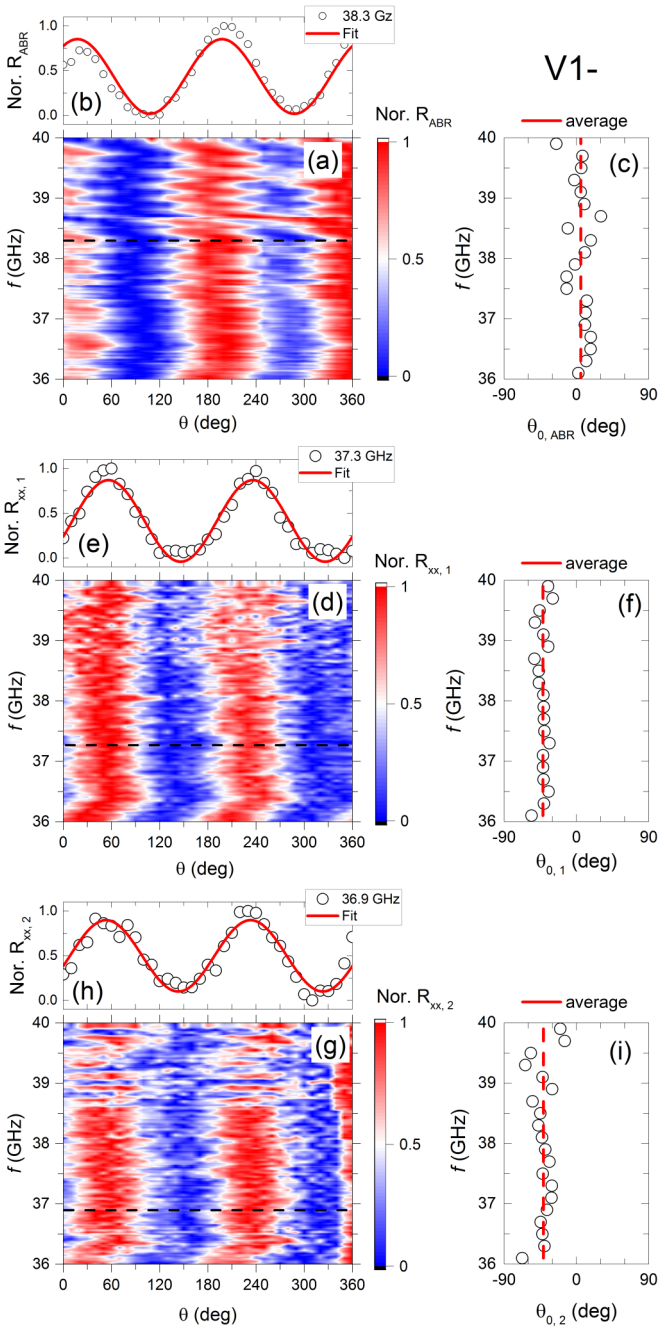

FIG. 2. The normalized resistance at the polarization angle (θ) response as a function of the radiation frequency, f, for the carbon resistor, $R_{\rm ABR}$ (top color plot: a), the diagonal resistance $R_{xx,1}$ for the $L/W = 1$ Hall bar section (center color plot: d), and the diagonal resistance $R_{xx,2}$ for the $L/W = 2$ section (bottom color plot: g), over a $36 \leqslant f \leqslant 40$ GHz band with $0^\circ \leqslant \theta \leqslant 360^\circ$ at the magnetic field corresponding to $V1-$. Panels (b), (e), and (h) illustrate the sinusoidal variation in resistance with θ at a given f. Panels (c), (f), and (i) show the phase shift θ_0 with f and the average value of θ_0. Here, θ_0 is extracted by fitting, at each frequency, the angular response exemplified in panels (b), (e), and (h); see the text. Parts (c), (f), and (i) imply a constant average phase shift at $V1-$.

roughly about $\theta = 0^\circ$, and this feature holds true with changing f. The sinusoidal variation of normalized $R_{\rm ABR}$ versus θ at $f = 38.3$ GHz [dashed black line in Fig. 2(a)] is displayed in Fig. 2(b). We fit the cosine square law [19,22,24–27], normalized $R_{\rm ABR}(\theta) = A + C\cos^2(\theta - \theta_{0,\rm ABR})$, to experimental data in order to extract $\theta_{0,\rm ABR}$, and all extracted $\theta_{0,\rm ABR}$ are plotted over $36 \leqslant f \leqslant 40$ GHz in Fig. 2(c). We average over the extracted $\theta_{0,\rm ABR}$ to obtain the average of $\theta_{0,\rm ABR}$, which is 5.3°, very close to $\theta = 0^\circ$. The 5.3° shift is attributed to the combined misalignments of the Hall bar, the carbon resistor, and the antenna. The standard deviation here is $\approx 13.0^\circ$.

Figure 2(d) shows a normalized $R_{xx,1}$ color plot of f versus θ. Similar to Fig. 2(a), it exhibits periodic strips with θ, which means the normalized $R_{xx,1}$ versus θ curve is sinusoidal, too. In Fig. 2(e), a cosine square law [19,22,24–27], normalized $R_{xx,1}(\theta) = A - C\cos^2(\theta - \theta_{0,1})$, serves to fit experimental data for the determination of $\theta_{0,1}$ [Fig. 2(e)]. The f versus $\theta_{0,1}$ curve and the average of $\theta_{0,1}$ (-41.8°) are illustrated in Fig. 2(f). Similarly, Figs. 2(g), 2(h), and 2(i) demonstrate a normalized $R_{xx,2}$ color plot, a normalized $R_{xx,2}$ versus θ sinusoidal curve, and f versus $\theta_{0,2}$ with $\theta_{0,2}$ average (-41.3°). Here, remarkably, the averages of $\theta_{0,1}$ and $\theta_{0,2}$ are very close to each other. If we compare the average of $\theta_{0,\rm ABR}$, $\theta_{0,1}$, and $\theta_{0,2}$, there is a perceptible difference between the ABR and the specimen. This implies that $\theta_{0,1}$ and $\theta_{0,2}$ reflect characteristic properties of the specimen. The approximate f-independence in Figs. 2(d) and 2(g) means θ_0 does not change very much with f.

Next, the f-sweep measurements are carried out at $P1-$. Figure 3(a) exhibits a normalized color plot of $R_{\rm ABR}$ versus f and θ. Similar to Fig. 2(a), periodic strips are observable and higher normalized $R_{\rm ABR}$ occurs near $\theta = 0$. Figure 3(b) indicates sinusoidal variation in normalized $R_{\rm ABR}$ versus θ. The $\theta_{0,\rm ABR}$ obtained by fitting to the cosine square law over $36 \leqslant f \leqslant 40$ GHz is plotted in Fig. 3(c), and the average of $\theta_{0,\rm ABR}$ is 13.3°. Since $V1-$ and $P1-$ occur at different magnetic fields [1–8,10–30], similar values for $\theta_{0,\rm ABR}$ at these two extrema suggest that the polarization hardly changes with B. The normalized $R_{xx,1}$ color plot [see Fig. 3(d)] depicts vertical stripes similar to that at $V1-$. Again at $P1-$, $\theta_{0,1}$ is extracted by fitting normalized $R_{xx,1}(\theta) = A + C\cos^2(\theta - \theta_{0,1})$, as shown in Fig. 3(e). The $\theta_{0,1}$ versus f trace is plotted in Fig. 3(f), and the average of $\theta_{0,1}$ (-41.8°) is indicated. Figure 3(g) displays a normalized $R_{xx,2}$ color plot, which looks different in comparison to $R_{xx,1}$ and suggests an f dependence. From fits to the cosine square law [see Fig. 3(h)] to the experimental data to extract $\theta_{0,2}$, distinct $\theta_{0,2}$ variation is observable over $36 \leqslant f \leqslant 38$ GHz, as shown in Fig. 3(i). A comparison of the standard deviations of $\theta_{0,\rm ABR}$, $\theta_{0,1}$, and $\theta_{0,2}$ shows that the standard deviation of $\theta_{0,2}$ (31.0°) is much larger than that of $\theta_{0,\rm ABR}$ (11.6°) and $\theta_{0,1}$ (10.0°).

For the sake of completeness, we extracted $\theta_{0,\rm ABR}$, $\theta_{0,1}$, and $\theta_{0,2}$ also over the remaining oscillatory extrema between $36 \leqslant f \leqslant 40$ GHz, and the results are summarized in Fig. 4. Figure 4(a) illustrates $\theta_{0,\rm ABR}$ as a function of f. It shows $\theta_{0,\rm ABR}$ extracted from the different oscillatory extrema are clustered together over $36 \leqslant f \leqslant 40$ GHz. Because the $\theta_{0,\rm ABR}$ appear f- and B-independent, we average over all the obtained $\theta_{0,\rm ABR}$ and report an overall average of $\theta_{0,\rm ABR} = 10.6^\circ$. This result confirms that one may use the carbon resistor as an

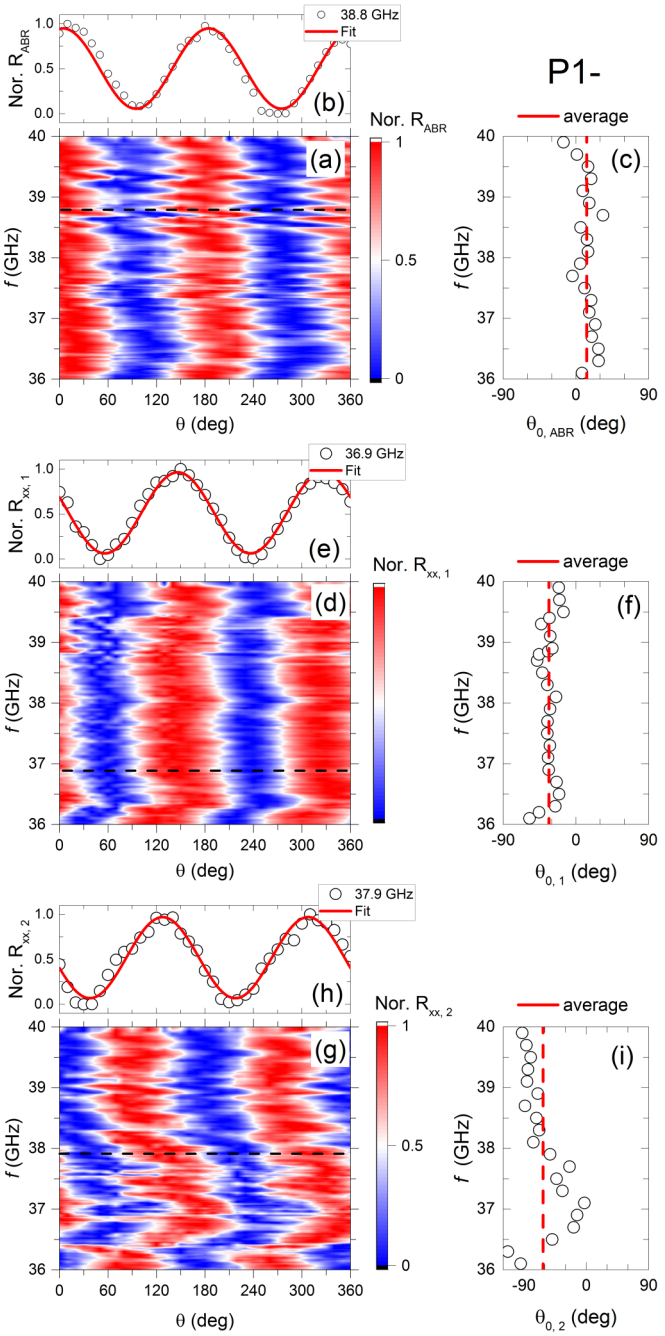

FIG. 3. At $P1-$, the normalized resistance at the polarization angle (θ) response is shown as a function of the radiation frequency, f, for the carbon resistor, R_{ABR} (top color plot: a), the diagonal resistance $R_{xx,1}$ for the $L/W = 1$ Hall bar section (center color plot: d), and the diagonal resistance $R_{xx,2}$ for the $L/W = 2$ section (bottom color plot: g), over a $36 \leqslant f \leqslant 40$ GHz band with $0^\circ \leqslant \theta \leqslant 360^\circ$. Panels (b), (e), and (h) illustrate the sinusoidal variation in resistance with θ at a given f. Panels (c), (f), and (i) show the phase shift θ_0 with f and the average value of θ_0. Here, θ_0 is extracted by fitting, at each frequency, the angular response exemplified in panels (b), (e), and (h); see text. The figure implies f-independence of $\theta_{0,\mathrm{ABR}}$ and $\theta_{0,1}$, but not in $\theta_{0,2}$ over $36 \leqslant f \leqslant 38$ GHz.

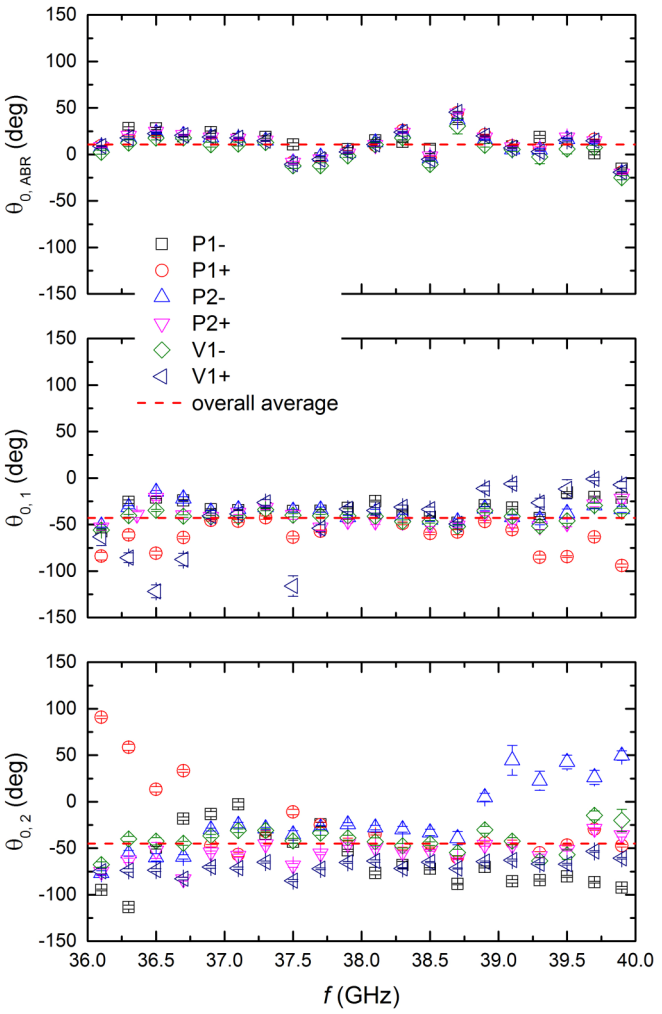

FIG. 4. (a) $\theta_{0,\mathrm{ABR}}$ as a function of f over $36 \leqslant f \leqslant 40$ GHz at all six oscillatory extrema: $P1+$, $V1+$, $P2+$, $P2-$, $V1-$, and $P1-$. Small, constant, and clustered, $\theta_{0,\mathrm{ABR}}$ are observed at different extrema. (b) $\theta_{0,1}$ as a function of f at all six oscillatory extrema. $\theta_{0,1}$ appear as for $\theta_{0,\mathrm{ABR}}$ and are relatively unaffected by f. (c) $\theta_{0,2}$ as a function of f at all six oscillatory extrema. The figure suggests that $\theta_{0,2}$ are more scattered than $\theta_{0,\mathrm{ABR}}$ and $\theta_{0,1}$, and are sensitive to f. The overall average values of $\theta_{0,1}$ and $\theta_{0,2}$ are approximately the same.

in situ detector of microwave polarization. The 10.6° shift from zero degrees, the expected value, might be caused by a minor combined misalignment of the Hall bar, the carbon resistor, and the microwave launcher. Figures 4(b) and 4(c) represent $\theta_{0,1}$ and $\theta_{0,2}$ versus f. The overall average is calculated by averaging over all $\theta_{0,1}$ and $\theta_{0,2}$ separately. At first glance, $\theta_{0,1}$ appear more clustered than $\theta_{0,2}$. In addition, some θ_0 exhibit a clear dependence on f, e.g., $\theta_{0,2}$ at $P2-$, and some do not, e.g., $\theta_{0,1}$ at $P2+$. To clarify the reason for this, we calculate the average ± standard deviation of θ_0 at each oscillatory extrema over $36 \leqslant f \leqslant 40$ GHz and list them in Table I. The table suggests that $\theta_{0,\mathrm{ABR}}$ and $\theta_{0,1}$ have nearly the same standard deviations at each oscillatory extrema, except for $V1+$. However, half of the extrema of $\theta_{0,2}$ manifest larger standard deviations than $\theta_{0,\mathrm{ABR}}$. This implies the possibility that the distinguishable f dependence in $\theta_{0,2}$ is larger than that in $\theta_{0,1}$. The overall standard deviations (averaging over

TABLE I. The average ± standard deviation of θ_0 at each oscillatory extrema over $36 \leqslant f \leqslant 40$ GHz is calculated. This comparison implies that $\theta_{0,2}$ has a larger standard deviation than $\theta_{0,\mathrm{ABR}}$ and $\theta_{0,1}$ over $36 \leqslant f \leqslant 40$ GHz. Also, the averages of $\theta_{0,1}$ and $\theta_{0,2}$ over all extrema differ significantly from the average of $\theta_{0,\mathrm{ABR}}$ over all extrema.

	$P1-$	$P1+$	$P2-$	$P2+$	$V1-$	$V1+$
$\theta_{0,\mathrm{ABR}}$	$13.3^\circ \pm 11.6^\circ$	$11.4^\circ \pm 13.9^\circ$	$10.7^\circ \pm 13.1^\circ$	$11.5^\circ \pm 14.1^\circ$	$5.3^\circ \pm 13.2^\circ$	$11.2^\circ \pm 14.3^\circ$
$\theta_{0,1}$	$-32.1^\circ \pm 10.2^\circ$	$-61.3^\circ \pm 16.3^\circ$	$-36.0^\circ \pm 8.5^\circ$	$-41.7^\circ \pm 9.7^\circ$	$-41.8^\circ \pm 6.6^\circ$	$-44.0^\circ \pm 35.0^\circ$
$\theta_{0,2}$	$-62.5^\circ \pm 31.0^\circ$	$-23.9^\circ \pm 41.3^\circ$	$-18.1^\circ \pm 37.2^\circ$	$-54.4^\circ \pm 12.4^\circ$	$-41.3^\circ \pm 13.1^\circ$	$-69.1^\circ \pm 7.3^\circ$

all standard deviations of θ_0) of $\theta_{0,\mathrm{ABR}} = 13.3^\circ$, $\theta_{0,1} = 14.4^\circ$, and $\theta_{0,2} = 23.7^\circ$ further prove that $\theta_{0,2}$ is more sensitive to f. However, surprisingly, the overall averages of $\theta_{0,1} = -42.8^\circ$ and $\theta_{0,2} = -44.9^\circ$ are remarkably close to each other and manifestly different from the overall average of $\theta_{0,\mathrm{ABR}}$.

III. DISCUSSION

In these experiments, the microwave launcher and the major axis of the Hall bar were aligned before the start of the experiments. Then, the relative rotation of the microwave polarization produced by the setup, as a function of frequency, was determined with the aid of a microwave power detector, as in previous studies [19,22,24–27]. The results showed that the standard error of incident microwave polarization orientation is $\approx 8.0^\circ$. However, there was still the possibility that the incident microwave polarization could be different close to the sample during measurement because the specimen included several metallic contacts and bonded gold wires that could influence the microwave polarization. The *in situ* measurements of the microwave polarization orientation by a carbon sensor close to the sample showed, however, that the overall average of $\theta_{0,\mathrm{ABR}} = 10.6^\circ$ is very close to 0°, and the standard deviation of $\theta_{0,\mathrm{ABR}} = 13.3^\circ$ is also within the measured standard error $\approx 8.0^\circ$ observed before the start of the experiment. This feature suggests good control of the microwave polarization orientation near the specimen during the measurement of the specimen. In addition, Figs. 4(b) and 4(c) illustrate that most of the $\theta_{0,1}$ and $\theta_{0,2}$ fall within $-75^\circ \leqslant \theta_0 \leqslant -25^\circ$. The significant θ_0 difference between the carbon resistor ($\theta_{0,\mathrm{ABR}}$) and the specimen ($\theta_{0,1}$ and $\theta_{0,2}$) confirms the preference of the specimen for microwave polarization at $\theta \approx -43.9^\circ$. Moreover, the overall averages of $\theta_{0,1}$ and $\theta_{0,2}$ appear to be almost identical. In other words, the average θ_0 does not appear to depend on f, B, and the length-to-width ratio of the Hall bar sections. This result differs from the previous work [19], and the difference is attributed here to the much higher mobility material used in the present experiment. Perhaps when the disorder is reduced in the higher mobility specimen, the dependence of the phase shift on the frequency, and the magnitude and direction of the magnetic field, are also reduced.

Recently, Mikhailov *et al.* proposed the "ponderomotive force" model to explain the origin of radiation-induced magnetotransport phenomena [50]. This theory was proposed as an alternative to preexisting approaches [32–37,39–48]. The suggestion of this theory is that the metallic contacts screening the incident electric field will induce a strong linearly polarized electric field near the contacts. The amplitude of the near-contact electric field perpendicular to the contact is supposed to be much larger than that of an incident electric field, while the amplitude of the near-contact electric field parallel with the contact is supposed to be much smaller than an incident electric field. Assume that the sample is subject to a linearly polarized electric field with an arbitrary orientation, then that electric field can be decomposed into $\vec{E}_{0x}$ (along the Hall bar) and $\vec{E}_{0y}$ (normal to the Hall bar). According to the theory, the probe contacts will lead to a near-contact electric field $\vec{E}_x$ (along the Hall bar) and $\vec{E}_y$ (normal to the Hall bar). Since $\vec{E}_x \ll \vec{E}_{0x}$ and $\vec{E}_y \gg \vec{E}_{0y}$ near the contacts, the resultant electric field that 2DES responds to near the contacts is $\approx \vec{E}_y$, and away from the contacts it is $\vec{E}_{0x} + \vec{E}_{0y}$. In comparing the two Hall bar sections with different length-to-width ratios, the influence of $\approx \vec{E}_y$ on the 2DES section remains constant because the contact geometry is the same, but $\vec{E}_{0x} + \vec{E}_{0y}$ will become more prominent when the separation of two probe contacts becomes larger in the larger length-to-width ratio section. In this case, the orientation of the resultant electric-field average over the long Hall bar section will approach the $\vec{E}_{0x} + \vec{E}_{0y}$ orientation. Thus, based on the "ponderomotive force" theory, one expects the phase shift θ_0 to change with the separation of two probe contacts. However, this experimental finding of the independence of the average phase shift on the length-to-width ratio of the Hall bar sections implies that experimental results do not follow expectations based on the "ponderomotive force" theory. In contrast, both the displacement theory and the radiation-driven electron orbit theory do not predict a dependence of the magnetotransport properties on the length-to-width ratio of the specimen [9,32,33,41,43–45,47–49,52,55,57,60], while none is observed here in the polarization angle phase shift. In this sense, there seems to be no inconsistency between experiment and those theories [9,32,33,41,43–45,47–49,52,55,57,60].

IV. CONCLUSION

In this work, the incident linear microwave polarization direction next to the sample has been independently determined by using an ABR carbon sensor. The observed small $\theta_{0,\mathrm{ABR}}$ could be attributed to the minor combined misalignment of the Hall bar, the ABR, and the antenna. The results also indicate that $\theta_{0,1}$ are more clustered with f than $\theta_{0,2}$, but they exhibit a nearly identical overall average, which differs substantially from $\theta_{0,\mathrm{ABR}}$. These features suggest the existence of a preferential microwave polarization angle for the specimen, and the independence of the average θ_0 on B, f, and the length-to-width ratio of the Hall bar

sections at oscillatory extrema over $36 \leqslant f \leqslant 40$ GHz in the investigated high-mobility material. The θ_0 independence of the length-to-width ratio of the Hall bar seems unexpected in light of the suggestions of the "'ponderomotive force" theory [50]. However, the observations are not inconsistent with the displacement theory and the radiation-driven electron orbit theory [9,32,33,41,43–45,47–49,52,55,57,60].

ACKNOWLEDGMENTS

Magnetotransport studies and H-C.L. at Georgia State University are supported by the U.S. Department of Energy, Office of Basic Energy Sciences, Material Sciences and Engineering Division under Grant No. DE-SC001762. R.L.S. is supported by the Army Research Office (ARO) under Contract No. W911NF-10-1-0450 and W911NF-15-1-0433.

[1] R. G. Mani, J. H. Smet, K. von Klitzing, V. Narayanamurti, W. B. Johnson, and V. Umansky, Nature (London) **420**, 646 (2002).

[2] M. A. Zudov, R. R. Du, L. N. Pfeiffer, and K. W. West, Phys. Rev. Lett. **90**, 046807 (2003).

[3] R. G. Mani, V. Narayanamurti, K. von Klitzing, J. H. Smet, W. B. Johnson, and V. Umansky, Phys. Rev. B **69**, 161306(R) (2004); **70**, 155310 (2004).

[4] R. G. Mani, J. H. Smet, K. von Klitzing, V. Narayanamurti, W. B. Johnson, and V. Umansky, Phys. Rev. Lett. **92**, 146801 (2004); Phys. Rev. B **69**, 193304 (2004).

[5] R. G. Mani, Physica E (Amsterdam) **22**, 1 (2004); **25**, 189 (2004); Int. J. Mod. Phys. B **18**, 3473 (2004); Appl. Phys. Lett. **85**, 4962 (2004); Phys. Rev. B **72**, 075327 (2005); Appl. Phys. Lett. **91**, 132103 (2007); Solid State Commun. **144**, 409 (2007); Physica E (Amsterdam) **40**, 1178 (2008).

[6] J. H. Smet, B. Gorshunov, C. Jiang, L. Pfeiffer, K. West, V. Umansky, M. Dressel, R. Meisels, F. Kuchar, and K. von Klitzing, Phys. Rev. Lett. **95**, 116804 (2005).

[7] A. Wirthmann, B. D. McCombe, D. Heitmann, S. Holland, K. J. Friedland, and C.-M. Hu, Phys. Rev. B **76**, 195315 (2007).

[8] S. A. Studenikin, A. S. Sachrajda, J. A. Gupta, Z. R. Wasilewski, O. M. Fedorych, M. Byszewski, D. K. Maude, M. Potemski, M. Hilke, K. W. West, and L. N. Pfeiffer, Phys. Rev. B **76**, 165321 (2007).

[9] O. E. Raichev, Phys. Rev. B **78**, 125304 (2008).

[10] R. G. Mani, Appl. Phys. Lett. **92**, 102107 (2008).

[11] A. T. Hatke, M. A. Zudov, L. N. Pfeiffer, and K. W. West, Phys. Rev. Lett. **102**, 066804 (2009).

[12] R. G. Mani, W. B. Johnson, V. Umansky, V. Narayanamurti, and K. Ploog, Phys. Rev. B **79**, 205320 (2009); Solid State Commun. **149**, 1531 (2009).

[13] O. M. Fedorych, M. Potemski, S. A. Studenikin, J. A. Gupta, Z. R. Wasilewski, and I. A. Dmitriev, Phys. Rev. B **81**, 201302(R) (2010).

[14] S. Wiedmann, G. M. Gusev, O. E. Raichev, A. K. Bakarov, and J. C. Portal, Phys. Rev. Lett. **105**, 026804 (2010).

[15] R. G. Mani, C. Gerl, S. Schmult, W. Wegscheider, and V. Umansky, Phys. Rev. B **81**, 125320 (2010); J. Phys. Soc. Jpn. **65**, 1751 (1996).

[16] A. N. Ramanayaka, R. G. Mani, and W. Wegscheider, Phys. Rev. B **83**, 165303 (2011).

[17] R. G. Mani, A. N. Ramanayaka, and W. Wegscheider, Phys. Rev. B **84**, 085308 (2011).

[18] R. G. Mani, A. Kriisa, and W. Wegscheider, Sci. Rep. **3**, 2747 (2013).

[19] A. N. Ramanayaka, R. G. Mani, J. Iñarrea, and W. Wegscheider, Phys. Rev. B **85**, 205315 (2012).

[20] R. G. Mani, A. N. Ramanayaka, T. Ye, M. S. Heimbeck, H. O. Everitt, and W. Wegscheider, Phys. Rev. B **87**, 245308 (2013).

[21] R. G. Mani and A. Kriisa, Sci. Rep. **3**, 3478 (2013).

[22] T. Ye, R. G. Mani, and W. Wegscheider, Appl. Phys. Lett. **102**, 242113 (2013); **103**, 192106 (2013); **105**, 191609 (2014).

[23] D. Konstantinov, Y. Monarkha, and K. Kono, Phys. Rev. Lett. **111**, 266802 (2013).

[24] A. N. Ramanayaka, T. Ye, H.-C. Liu, W. Wegscheider, and R. G. Mani, Physica B **453**, 43 (2014).

[25] T. Ye, H.-C. Liu, W. Wegscheider, and R. G. Mani, Phys. Rev. B **89**, 155307 (2014).

[26] H.-C. Liu, T. Ye, W. Wegscheider, and R. G. Mani, J. Appl. Phys. **117**, 064306 (2015).

[27] T. Ye, H.-C. Liu, Z. Wang, W. Wegscheider, and R. G. Mani, Sci. Rep. **5**, 14880 (2015).

[28] A. D. Chepelianskii, J. Laidet, I. Farrer, D. A. Ritchie, K. Kono, and H. Bouchiat, Phys. Rev. B **90**, 045301 (2014).

[29] Z. Wang, R. L. Samaraweera, C. Reichl, W. Wegscheider, and R. G. Mani, Sci. Rep. **6**, 38516 (2016).

[30] A. D. Chepelianskii, M. Watanabe, K. Nasyedkin, K. Kono, and D. Konstantinov, Nat. Commun. **6**, 7210 (2015).

[31] W. Zhou, H. M. Yoo, S. Prabhu-Gaunkar, L. Tiemann, C. Reichl, W. Wegscheider, and M. Grayson, Phys. Rev. Lett. **115**, 186804 (2015).

[32] A. C. Durst, S. Sachdev, N. Read, and S. M. Girvin, Phys. Rev. Lett. **91**, 086803 (2003).

[33] V. Ryzhii and R. Suris, J. Phys.: Condens. Matter **15**, 6855 (2003).

[34] X. L. Lei and S. Y. Liu, Phys. Rev. Lett. **91**, 226805 (2003).

[35] A. A. Koulakov and M. E. Raikh, Phys. Rev. B **68**, 115324 (2003).

[36] A. V. Andreev, I. L. Aleiner, and A. J. Millis, Phys. Rev. Lett. **91**, 056803 (2003).

[37] P. H. Rivera and P. A. Schulz, Phys. Rev. B **70**, 075314 (2004).

[38] S. A. Mikhailov, Phys. Rev. B **70**, 165311 (2004).

[39] A. Auerbach, I. Finkler, B. I. Halperin, and A. Yacoby, Phys. Rev. Lett. **94**, 196801 (2005).

[40] J. Iñarrea and G. Platero, Phys. Rev. Lett. **94**, 016806 (2005).

[41] X. L. Lei and S. Y. Liu, Phys. Rev. B **72**, 075345 (2005).

[42] I. A. Dmitriev, M. G. Vavilov, I. L. Aleiner, A. D. Mirlin, and D. G. Polyakov, Phys. Rev. B **71**, 115316 (2005).

[43] J. Dietel, Phys. Rev. B **73**, 125350 (2006).

[44] J. Iñarrea and G. Platero, Phys. Rev. B **76**, 073311 (2007).

[45] J. Iñarrea and G. Platero, Appl. Phys. Lett. **93**, 062104 (2008).

[46] S. Wang and T.-K. Ng, Phys. Rev. B **77**, 165324 (2008).

[47] X. L. Lei and S. Y. Liu, Appl. Phys. Lett. **94**, 232107 (2009).

[48] J. Iñarrea, R. G. Mani, and W. Wegscheider, Phys. Rev. B **82**, 205321 (2010).
[49] J. Iñarrea and G. Platero, Phys. Rev. B **84**, 075313 (2011).
[50] S. A. Mikhailov, Phys. Rev. B **83**, 155303 (2011).
[51] A. D. Chepelianskii, J. Laidet, I. Farrer, H. E. Beere, D. A. Ritchie, and H. Bouchiat, Phys. Rev. B **86**, 205108 (2012).
[52] J. Iñarrea, Appl. Phys. Lett. **100**, 242103 (2012).
[53] X. L. Lei and S. Y. Liu, Phys. Rev. B **86**, 205303 (2012).
[54] A. Kunold and M. Torres, Physica B **425**, 78 (2013).
[55] J. Iñarrea, J. Appl. Phys. **113**, 183717 (2013).
[56] O. V. Zhirov, A. D. Chepelianskii, and D. L. Shepelyansky, Phys. Rev. B **88**, 035410 (2013).
[57] X. L. Lei and S. Y. Liu, J. Appl. Phys. **115**, 233711 (2014).
[58] A. Yar and K. Sabeeh, J. Phys.: Condens. Matter **27**, 435007 (2015).
[59] V. G. Ibarra-Sierra, J. C. Sandoval-Santana, J. L. Cardoso, and A. Kunold, Ann. Phys. (NY) **362**, 83 (2015).
[60] O. E. Raichev, Phys. Rev. B **91**, 235307 (2015).